Taylor & Francis
Taylor & Francis Group

Use of normalized difference built-up index in automatically mapping urban areas from TM imagery

Y. ZHA

College of Geographical Sciences, Nanjing Normal University, Nanjing 210097, China; e-mail: yzha@njnu.edu.cn

J. GAO*

School of Geography and Environmental Science, University of Auckland, Private Bag 92019, Auckland, New Zealand; e-mail: jg.gao@auckland.ac.nz

and S. NI

College of Geographical Sciences, Nanjing Normal University, Nanjing 210097

Abstract. Remotely sensed imagery is ideally used to monitor and detect land cover changes that occur frequently in urban and peri-urban areas as a consequence of incessant urbanization. It is a lengthy process to convert satellite imagery into land cover map using the existing methods of manual interpretation and parametric image classification digitally. In this paper we propose a new method based on Normalized Difference Built-up Index (NDBI) to automate the process of mapping built-up areas. It takes advantage of the unique spectral response of built-up areas and other land covers. Built-up areas are effectively mapped through arithmetic manipulation of re-coded Normalized Difference Vegetation Index (NDVI) and NDBI images derived from TM imagery. The devised NDBI method was applied to map urban land in the city of Nanjing, eastern China. The mapped results at an accuracy of 92.6% indicate that it can be used to fulfil the mapping objective reliably. Compared with the maximum likelihood classification method, the proposed NDBI is able to serve as a worthwhile alternative for quickly and objectively mapping built-up areas.

1. Introduction

Land covers in urban areas tend to change more drastically over a short period of time than elsewhere because of incessant urbanization. Urbanization has led land covers to change especially frequently in peri-urban areas in China as a result of rapid economic development. These changes are ideally monitored and detected from remotely sensed images as they are relatively up-to-date and give a panoramic view.

Remote sensing materials in the form of aerial photographs and satellite images are usually converted into useful information such as land cover maps using two

---

*Corresponding author.

conventional methods: manual interpretation and computer-assisted digital pro-
cessing. During manual interpretation analogue photographs or satellite images are
visually interpreted and the results delineated directly on the photographs or images
or on tracing paper placed over them. Manual interpretation of Landsat 70 mm film
images could produce small-scale (e.g. 1:250 000) maps with an acceptable semantic
accuracy (89%), especially if a high level of generalization was intended (Lo 1981).
Visual interpretation of space shuttle Large Format Camera (LFC) photographs and
National High Altitude Photographs (NHAP) of Boston resulted in urban land use
and land cover types mapping 65% and 70%, respectively, from LFC and NHAP
photographs correctly at level III of the US Geological Survey (USGS) classification
scheme (Lo and Noble 1990).

Remotely sensed data have become increasingly available in a digital form,
allowing for their computer-assisted interpretation and processing. Irrespective of
the specific form of the remote sensing materials, manual interpretation is tedious,
time-consuming, and the interpreted results highly subjective to the image analyst.
By comparison, supervised classification is much faster and requires far less human
intervention. Lo (1981) found that a computer-assisted method of analysis of Landsat
data permits more detailed urban land use information to be extracted, but at an
accuracy of only 69%. A critical limitation with this method is that only the spectral
information of image pixels is taken advantage of for the classification. Therefore,
other image elements such as location, shape, shadow are ignored. Understandably,
the classification accuracy is rather low. As a matter of fact, automatic classification
of satellite images for urban areas is a difficult task to achieve at a high accuracy
level due to the diverse range of covers. Gao and Skillcorn (1998) achieved an overall
accuracy of 76.2% and 81.4% from winter and summer Système Probatoire de
l'Observation de la Terre (SPOT) sensor data, respectively, in generating detailed
land cover maps at the urban–rural fringe of Auckland, New Zealand, at level II
of the Anderson scheme. Treitz *et al.* (1992) achieved an overall Kappa coefficient
of 82.2% for training area data and 70.3% for the entire SPOT High Resolution
Visible (HRV) data of the rural–urban fringe of Toronto, Canada. In order to
improve the accuracy, Stuckens *et al.* (2000) used a hybrid segmentation procedure
to integrate contextual information. Overall accuracy of the optimal classification
technique was 91.4% for a level II classification (10 classes) with a K(e) of 90.5%.

The results automatically classified from satellite data, to some extent, are still
subject to the characteristics of the selected training samples. Their location, size
and representativeness all directly govern the reliability of the subsequently classified
results. The classification is slowed down by the requirement of selecting training
samples for all those covers to be mapped. Therefore, conventional methods of
parametric classification tend to be slow as a result of the need to select quality
training samples.

Considerable efforts have gone into simplifying the process of automatically
mapping land covers, such as using indices. One of the commonly used indices is
the Normalized Difference Vegetation Index (NDVI). This index takes advantage of
the unique shape of the reflectance curve of vegetation, and has been widely used
for mapping vegetation on the global scale from the Advanced Very High Resolution
Radiometer (AVHRR) data. For example, Achard and Estreguil (1995) used multi-
temporal AVHRR mosaics for tropical forest discrimination and mapping. Other
applications of NDVI include mapping of the surfaces affected by large forest
fires (Fernandez *et al.* 1997), assessment of the status of agricultural lands (Lenney

et al. 1996), derivation of snow cover products (Slater *et al.* 1999), discrimination of areas affected by volcanic eruption (Kerdiles and Diaz 1996) and so on. Multi-temporal NDVI data were also classified to characterize phenological responses on a spatially dissected landscape (Fleischmann and Walsh 1991) and to monitor dynamic parameters of vegetation (Azzali and Menenti 2000).

In addition to NDVI, Normalized Difference Snow Index (NDSI) has been devised from Landsat Thematic Mapper (TM) bands 2 and 5 to map glaciers (Sidjak and Wheate 1999). This index is based on the difference between strong reflection of visible radiation and near total absorption of middle infrared wavelengths by snow (Hall *et al.* 1995). It is effective in distinguishing snow from similarly bright soil, vegetation and rock, as well as from clouds (Dozier 1989).

Unlike NDSI, Normalized Difference Water Index (NDWI) has been developed to delineate open water features and enhance their presence in remotely sensed imagery based on reflected near-infrared radiation and visible green light. NDWI may allow turbidity of waterbodies to be estimated from remotely sensed data (McFeeters 1996). NDWI is sensitive to changes in liquid water content of vegetation canopies. It is complementary to, but not a substitute for NDVI (Gao 1996).

In this study we propose a new and simple method for the rapid and accurate mapping of urban areas. This method is based on the combinational use of NDBI and NDVI. The mapping is accomplished through arithmetic manipulations and recoding of NDBI and NDVI images derived from a 1997 TM image. This method does not involve any subjective human intervention in the mapping process. The effectiveness of this method was tested through the mapping of urban areas in the Chinese City of Nanjing. Comparison of the results obtained using this method with the manually interpreted ones demonstrates that it is highly reliable. This method also produces very accurate results more efficiently than the supervised classification method.

2. Study area

The study area is largely the urban area of Nanjing City, East China, located at $118°\,47'\,E$ and $32°\,04'\,N$ in the lower reaches of the Yangtze River (figure 1). Most of the urban areas lie to the south of the river. Situated in the Yangtze River delta, the city has a mostly gentle topography with little relief. Hilly areas are found in the outskirts. The tallest mountain of Zijin is 448 m above sea level. Thus, little topographic shadow is present on the satellite imagery. Apart from the Yangtze River, another major waterbody is a recreational lake next to the mountain.

As the capital of Jiangsu province, Nanjing has a total area of $976\,km^2$. Land covers present in this area are mainly urban residential, commercial and industrial. Woodland is found in the adjacent mountainous areas. Natural vegetation occurs in the form of mixed coniferous trees. Artificially planted trees are mostly deciduous. In addition, there is farmland in the surrounding rural areas. Rice, wheat, vegetable oil seed, as well as vegetables are cultivated throughout the year. Some crop fields at the early stage of their growth may appear as barren on the TM image. Due to rapid economic development, farmland adjacent to the urban periphery has been converted to urban uses over the last two decades. Therefore, it is necessary from time to time to monitor these changes from satellite imagery.

3. Data and processing

Landsat TM imagery was used in this study because of its finer spectral resolution than other commonly used images such as SPOT and Multi-Spectral Scanner (MSS).
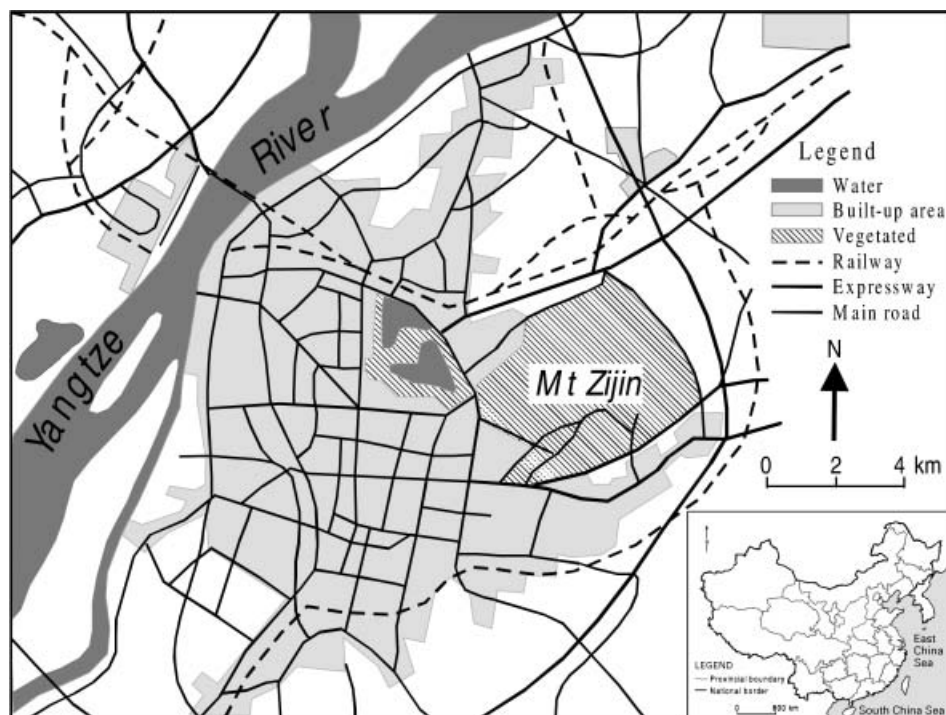
Figure 1.   Location of the study area.

A full-scene TM imagery (5728 rows by 6920 columns) of 18 October 1997 was acquired with all seven bands. The image quality was rather good with no cloud cover over the study area. A topographic map of 1:50 000 was also acquired; published in 1970, it has the Gausse-Krügel coordinate system with ground coordinates indicated by 1 km grids.

All image processing and analyses were carried out in ER Mapper® in the Windows NT (version 6.0) environment. A sub-area of 1401 rows by 1408 columns was initially subset from the raw image. False colour composites were formed using various band combinations and displayed on the screen to differentiate diverse types of land covers. In the end the standard composite of bands 2, 3 and 4 (figure 2) was selected. The subset image was geometrically rectified using eight ground control points. They were intersections of river channels, turns and intersections of roads with themselves and with river channels. Their ground coordinates in the Gausse-Krügel coordinate system were read from the topographic map. The residuals at these control points ranged from 0.15–1.75 pixels. Once this accuracy was considered accurate, the original image was projected linearly to the new system. During projection transformation the image was resampled to the same spatial resolution using the nearest neighbour method. Afterwards, the image, which did not conform to any regular orientation, was subset once more to 800 rows by 800 columns (figure 2).

4.   NDBI

Figure 2 is the standard false colour composite (TM4—red, TM3—green, TM2—blue) on which various surface covers (e.g. built-up, woodland, farmland, barren and water) are clearly distinguishable. Through repeatedly clicking on the representative
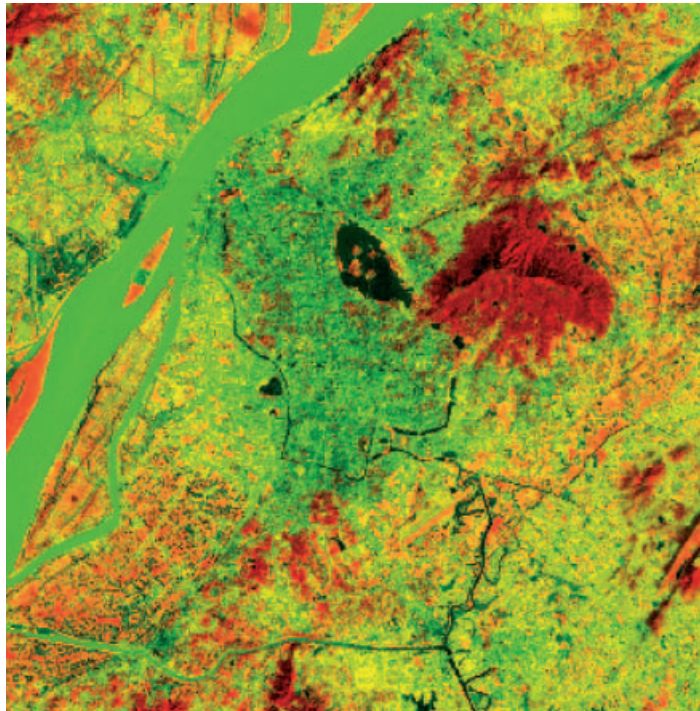
Figure 2.   False colour composite of TM bands 4 (red), 3 (green) and 2 (blue). Typical land
              covers are urban (bluish yellow), woodland (dark red), barren (yellow), river (green),
              lakes (dark), and farmland (orange). Image size: 800 by 800 pixels.

pixels of each of these covers, their values in all seven bands are averaged and
displayed graphically in figure 3. This profile illustrates that their spectral disparity
is the largest in bands 3, 4 and 5. An examination of the minimum, maximum and
standard deviation of each of the covers in the seven TM bands (table 1) confirms
the same conclusion. Namely, these values are most distinctive from one another for
each cover in bands 3, 4 and 5. Therefore, they are the most useful bands from which
some of the land covers may be potentially differentiated spectrally. Rivers and lakes
have a similar shape of profile. Their Digital Number (DN) value is markedly lower
in the fourth and fifth bands. They experience a sharp rise in reflectance in band 6,
but a low reflectance in band 7. The curve for rivers lies above that for lakes because
they are laden with more silt.

   A close scrutiny of figure 3 reveals that except for barren, vegetation (woodland
and farmland) has a higher reflectance on band 4 than other covers. Moreover, its
value on band 4 still exceeds those on band 3. By comparison, all the non-vegetative
categories have a smaller DN on band 4 than 3. Therefore, the subtraction of band
3 from band 4 will result in positive DNs for vegetation pixels only. The afore-
mentioned relationships exist for the minimum and maximum DNs as well (table 1).
This outcome allows broad vegetative covers to be distinguished easily. This
processing is commonly referred to as NDVI (equation 1).

$$NDVI = (Band\ 4 - band\ 3)/(band\ 4 + band\ 3) \tag{1}$$

   In order to facilitate the subsequent processing, the derived NDVI image was
recoded with 254 for all pixels having positive indices (vegetation) and 0 for all
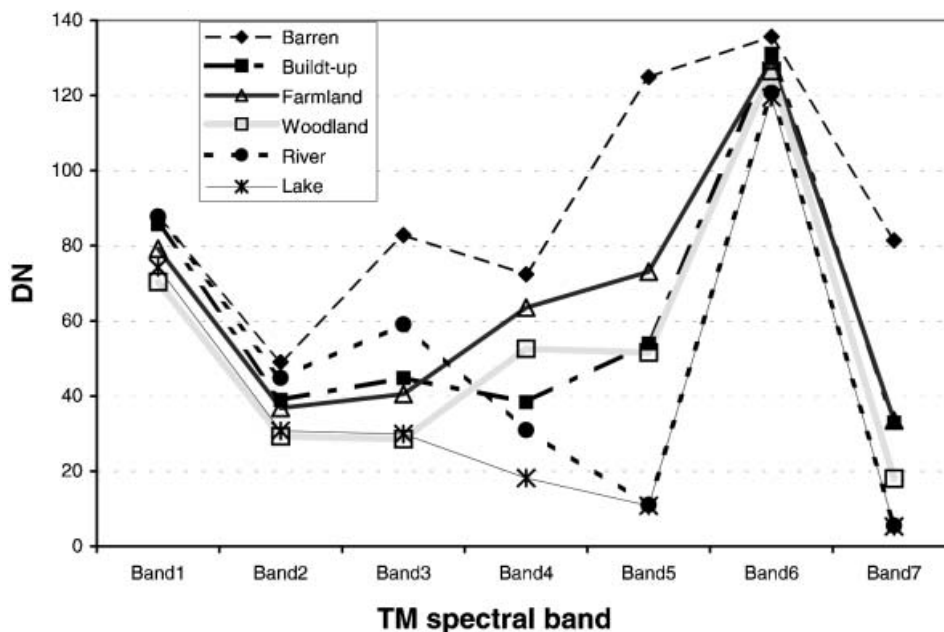remaining pixels of negative indices (table 2).

Figure 3. Spectral profiles of six typical land covers in the study area.

Table 1. Minimum, maximum and standard deviation of DNs of the six covers in the seven spectral TM bands.

TM spectral band		1	2	3	4	5	6	7
Built-up	Minimum	79	33	35	25	29	125	15
	Maximum	96	49	61	51	82	134	53
	Standard deviation	4.1	2.9	4.7	4.4	9	1.6	6.6
Barren	Minimum	82	46	70	66	103	132	65
	Maximum	94	51	98	79	154	143	101
	Standard deviation	4.3	1.8	11.8	5.6	22.9	4.4	15.7
Farmland	Minimum	76	33	34	41	55	128	20
	Maximum	91	43	56	79	103	131	57
	Standard deviation	2.4	2.1	3.5	8.2	9.5	0.9	6
Woodland	Minimum	67	26	25	38	41	124	13
	Maximum	76	35	39	59	70	130	34
	Standard deviation	1.7	1.4	2.1	3.5	6	1.2	3.4
River	Minimum	85	42	54	28	8	119	2
	Maximum	91	47	63	35	18	123	9
	Standard deviation	1.4	1.1	1.6	1.5	1.6	0.6	1.4
Lake	Minimum	71	29	27	17	9	118	2
	Maximum	78	33	32	20	13	121	8
	Standard deviation	1.6	0.8	1.1	0.8	1.2	0.8	1.3

Built-up areas and barren land experience a drastic increment in their reflectance from band 4 to band 5 while vegetation has a slightly larger or smaller DN value on band 5 than on band 4 (figure 3). This pace of increment greatly exceeds that of any other covers. The minimum and maximum DNs in band 4 are much smaller than those in band 5 for the same cover. The standardized differentiation of these

Table 2. Pixel values of representative land covers after differencing and binary recoding.

	Built-up	Barren	Woodland	Farmland	Rivers	Lakes
NDVI	0	0	254	254	0	0
NDBI	254	254	254 or 0	254 or 0	0	0
NDBI-NDVI	254	254	0 or −254	0 or −254	0	0

two bands (equation 2) will result in close to 0 for woodland and farmland pixels, negative for waterbodies, but positive values for built-up pixels, enabling the latter to be separated from the remaining covers.

$$NDBI = (TM5 - TM4)/(TM5 + TM4) \qquad (2)$$

The derived NDBI image was then recoded to create a binary image. The resultant ratio was assigned a new value of 0 if the input pixel had a negative index or 254 if its input index was larger than 0 (table 2). The spectral profiles in figure 3 suggest that the ratio for vegetative covers can be larger or smaller than 0, depending upon pixels in the surrounding environs. While many vegetative pixels may have been coded 0 correctly in the output binary image, this handling cannot effectively ensure that all vegetative pixels will receive the new value of 0. In order to avoid mistakenly grouping those vegetative pixels into the built-up category, a further step of processing is imperative. According to the results in table 2, subtraction of the recoded NDVI image from the recoded NDBI image will lead to only built-up and barren pixels having positive values while all other covers have a value of 0 or −254, thus allowing built-up areas to be mapped automatically. Through three arithmetic manipulations of TM bands 3, 4 and 5 followed by recoding, it is thus possible to differentiate urban areas (including barren land). In order to enhance the appearance of the final difference image, the derived urban built-up image was spatially filtered using the median filter with a window of 5 pixels by 5 pixels (figure 4). The filtered image was vectorized and later overlaid with the original colour composite to check for its spatial accuracy.

5.   Results
5.1. *NDBI-derived result and its accuracy*
Since this study concentrates on the mapping of built-up areas, all the mapped land covers are categorized into only two groups, built-up and all others. There are 166 180 built-up pixels in the study area, or an area of 15 403.148 ha (each pixel is 30.445 m by 30.445 m in dimension). Built-up areas account for nearly 26% of the entire study area. As implied previously, no further attempt was made to differentiate the specific uses of these areas.

The accuracy of the mapped built-up areas was assessed both spatially and aspatially. The spatial discrepancy between the mapped and actual boundaries of built-up areas is illustrated graphically in figure 5. It shows that the vectorized boundary of the mapped built-up areas matches closely with the actual border of built-up areas in this part of the image. In order to provide a quantitative assessment of the accuracy for the entire urban area, 68 pixels were randomly selected from the mapped results (figure 4). Their genuine identity on the ground was verified under the guidance of a global positioning system (GPS) receiver in the field according to their coordinates. It was found that of these checkpoints, 63 were correctly mapped
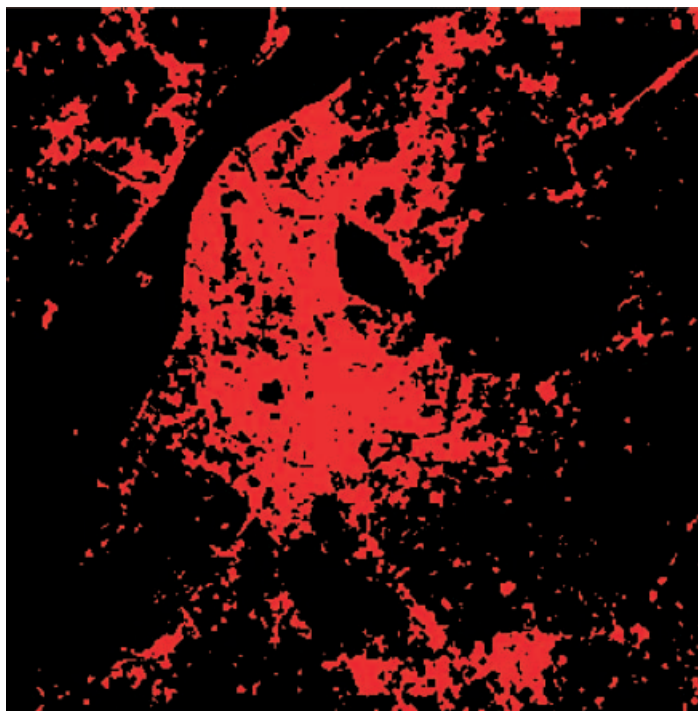
Figure 4.   Results of automatically mapped urban land use after spatial filtering with a
window size of 5 pixels by 5 pixels.

as urban areas, resulting in an accuracy of 92.6%. Of the five misclassified pixels, three were fallow land, one denudated rock and one sandy beach.

Aspatially, the area of 15 403.148 ha derived from the proposed NDBI method closely resembles the area of 14 300 ha that was obtained from manual measurement of a 1995 topographic map at a scale of 1:10 000. These two figures differ from each other by only 1103 ha, or less than 8% in relative terms. The apparent factor that may explain the discrepancy is rapid urbanization. Since the photographs used to generate the topographic map were taken, the urban area in Nanjing has expanded, resulting in a larger built-up area on the 1997 satellite image. In this sense, the mapped result is more current than the map-derived one.

The built-up areas have also been measured manually from the false colour composite. The manual result of 15 061.958 ha is highly similar to the NDBI-derived 15 403.148 ha. The two sets of result have a discrepancy of 341 ha or 2%. This discrepancy is explained by the fact that barren land is not included in the manual result. Barren land in the form of beaches, mudflats, rocks (both denudated and quarries), fallow land and transitional areas were not mapped as separate covers in the NDBI method. Due to their spectral proximity to built-up areas, they have been lumped together with built-up areas in this study. Since these covers make up a tiny portion of the study area, such a handling will not degrade the mapping accuracy of built-up areas considerably.

5.2. *Comparison with maximum likelihood method*

In order to assess the performance of the proposed NDBI method, the original TM imagery with all seven bands was classified using the conventional parametric
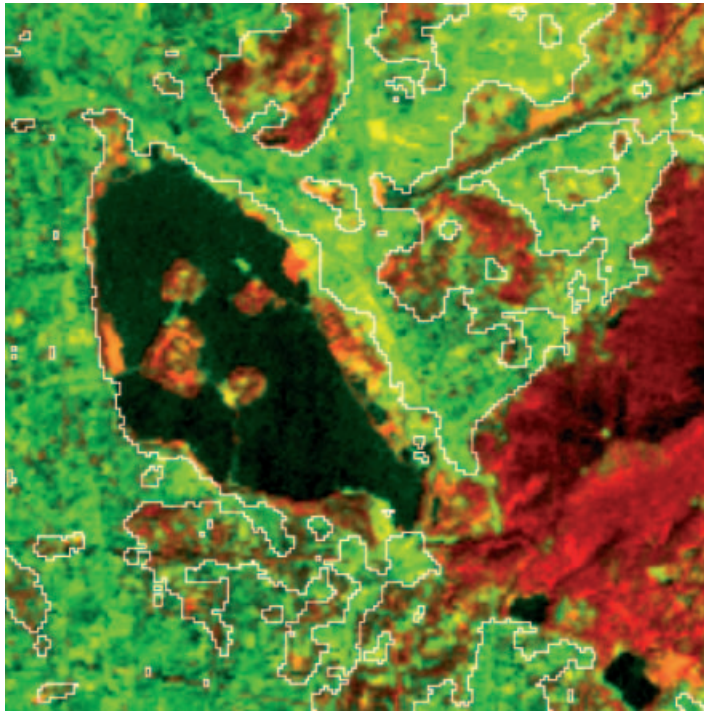
Figure 5. The agreement between built-up areas and the vectorized boundaries of filtered built-up areas on the false colour composite (an enlargement). Refer to figure 2 for the colour codes.

classification method (maximum likelihood) in which five classes of land covers (woodland, built-up areas, lakes, rivers and farmland) were mapped. Since barren land in the form of beaches, mudflats, rocks (both denudated and quarry) and fallow land is so subordinate within the study area, it has been ignored in the mapping. In total, the image was classified seven times. During each trial both the size of training samples and their location were varied. The results (table 3) indicate that the built-up areas mapped with the maximum likelihood method vary enormously from 10 to 319 320 pixels. The area of other covers fluctuates with each trial, as well. There is no definite relationship between the size of training samples and the classified area for a given cover category. The worst trial appears to be number 6 in which only 13 built-up pixels are classified, much less than the number of input pixel (112). No pixels in the other three categories are classified at all. Such an utterly unrealistic result is due probably to the poor quality of the training samples. These figures at least confirm that the results derived from supervised classification are not quite objective.

The classified built-up areas closest to their manually derived counterpart are at 195 519 pixels, or 18 123 ha. This result deviates from the manual one by 3061 ha. In other trials the supervised method consistently overestimates built-up areas. Therefore, the proposed NDBI method is superior to supervised classification. It may be argued that the inferior performance of the maximum likelihood method is partially contributed by the fact that built-up areas were classified into one single category. Other non-urban areas that share a similar spectral response with built-up areas, such as

Table 3.   Results of maximum likelihood classification using various training sample sizes. Samples were selected from the standard colour composite. Classification was carried out using all seven bands.

		Farmland	Lakes	Rivers	Built-up	Woodland
First trial	Sample size	640	400	560	576	576
	No. of pixels	284 659	3834	42 560	280 447	28 500
	Hectare	26 385	355	3945	25 995	2642
Second trial	Sample size	368	304	400	336	336
	No. of pixels	267 574	2885	42 231	314 727	12 583
	Hectare	24 801	267	3914	29 172	1166
Third trial	Sample size	176	192	256	160	256
	No. of pixels	262 276	3014	38 832	319 320	16 558
	Hectare	24 310	279	3599	29 598	1535
Fourth trial	Sample size	112	96	144	96	128
	No. of pixels	0	7	86 708	10	553 275
	Hectare	0	1	8037	1	51 282
Fifth trial	Sample size	128	96	128	144	128
	No. of pixels	63 604	7	14 384	195 519	366 486
	Hectare	5895	1	1333	18 123	33 969
Sixth trial	Sample size	80	112	80	112	128
	No. of pixels	0	0	0	13	639 987
	Hectare	0	0	0	1	59 320
Seventh trial	Sample size	48	64	64	64	80
	No. of pixels	283 296	4287	43 417	260 271	48 729
	Hectare	26 259	397	4024	24 124	4517

Note: training samples are also varied in their locations.

transitional areas and beaches, were not classified as separate groups. Certainly, the accuracy would be much higher had built-up areas first classified as subgroups that were merged in a post-classification session. This, undoubtedly, will prolong the already time-consuming process of supervised classification.

6.   Conclusions and discussion

This proposed NDBI method is able to map built-up areas at an accuracy level of 92.6%. The results mapped using NDBI are highly comparable to those from manual interpretation in quantity. The two sets of results differ from each other by 2% and closely match each other spatially, as well. In comparison with supervised classification, NDBI enables built-up areas to be mapped at a higher degree of accuracy and objectivity. The absence of training samples from the mapping makes subjective intervention from the human analyst redundant. This means that the same results can be derived regardless of the analyst or how many times the mapping is repeated. The redundancy also considerably expedites the mapping process that can be accomplished by direct subtractions of original spectral bands. Through arithmetic manipulation of TM bands and simple recoding of the intermediate images, NDBI does not require complex mathematical computation. It is concluded that the proposed NDBI is much more effective and advantageous in mapping general built-up areas than the maximum likelihood method. It can serve as a worthwhile alternative for quickly mapping urban land.

The assumption underlying the NDBI method is the spectral reflectance of urban areas in TM5 exceeding that in TM4. This method will generate valid results so

long as this assumption is not violated. Because the reflectance of urban areas exhibits little seasonality, this method is not prone to its impact. However, its performance may be adversely affected indirectly by the presence of other covers whose reflectance is seasonal, such as forest. This problem may be overcome with the selection of images recorded when defoliation is minimal or non-existent. The mixture of built-up areas with barren farmland may be overcome with the use of an image taken when vegetative cover is at its maximum.

Nevertheless, this proposed method does have a number of limitations. First of all, it can map only broad urban land covers. For instance, urban industrial, commercial and residential areas are impossible to be separated. This, however, may not prove to be a liability in most Chinese cities where they are highly intermixed spatially. They are difficult to be satisfactorily mapped even using the conventional supervised classification method anyway. Secondly, the NDBI method is unable to separate urban areas from barren (e.g. sandy beaches) because both of them have a similar spectral response in all TM bands. This limitation may be overcome with the use of spatial knowledge, as the latter is located next to water. Another remedial method is to select an image recorded in a season when the water level is so high that sand beaches are submerged under water. By comparison, the effect of drought on the performance of the NDBI method is more difficult to counteract. The loss of moisture from soil and disappearance of vegetation as a result of drought will assimilate the spectral characteristics of both urban and agricultural areas, debilitating the validity of the proposed method. Predictably, the reliability of this method is lowered in mapping peripheral urban areas where barren or fallow land is widespread. Thirdly, the universality of this proposed method needs to be tested in other geographic areas. The success of the proposed method lies in the NDVI value of vegetation being larger than 0. However, the spectral response of vegetation varies from location to location due to different kinds of species and nature of underlying soil and moisture conditions. Besides, the response pattern for vegetation varies with its density. Under these circumstances it is uncertain whether vegetative NDVI value still exceeds 0. It is speculated that the specific reflectance values may vary with these conditions, but the general pattern of the spectral response of vegetation in all seven TM bands will remain identical, ensuring a positive NDVI value and thus maintaining the validity of the method.

References

ACHARD, F., and ESTREGUIL, C., 1995, Forest classification of Southeast Asia using NOAA AVHRR data. *Remote Sensing of Environment*, **54**, 198–208.

AZZALI, S., and MENENTI, M., 2000, Mapping vegetation–soil–climate complexes in southern Africa using temporal Fourier analysis of NOAA AVHRR NDVI data. *International Journal of Remote Sensing*, **21**, 973–996.

DOZIER, J., 1989, Spectral signature of Alpine snow cover from the Landsat Thematic Mapper. *Remote Sensing of Environment*, **28**, 9–22.

FERNANDEZ, A., ILLERA, P., and CASANOVA, J. L., 1997, Automatic mapping of surfaces affected by forest fires in Spain using AVHRR NDVI composite image data. *Remote Sensing of Environment,* **60**, 153–162.

FLEISCHMANN, C. G., and WALSH, S. J., 1991, Multi-temporal AVHRR digital data: an approach for landcover mapping of heterogeneous landscapes. *Geocarto International*, **6**, 5–20.

GAO, B. C., 1996, NDWI—a normalized difference water index for remote sensing of vegetation liquid water from space. *Remote Sensing of Environment*, **58**, 257–266.

GAO, J., and SKILLCORN, D., 1998, Capability of SPOT XS data in producing detailed land cover maps at the urban–rural periphery. *International Journal of Remote Sensing*, **19**, 2877–2891.

HALL, D. K., RIGGS, G. A., and SALOMONSON, V. V., 1995, Development of methods for mapping global snow cover using Moderate Resolution Imaging Spectroradiometer data. *Remote Sensing of Environment*, **54**, 127–140.

KERDILES, H., and DIAZ, R., 1996, Mapping of the volcanic ashes from the 1991 Hudson eruption using NOAA–AVHRR data. *International Journal of Remote Sensing*, **17**, 1981–1995.

LENNEY, M. P., WOODCOCK, C. E., COLLINS, J. B., and HAMDI, H., 1996, The status of agricultural lands in Egypt: the use of multitemporal NDVI features derived from Landsat TM. *Remote Sensing of Environment*, **56**, 8–20.

LO, C. P., 1981, Land use mapping of Hong Kong from Landsat images. An evaluation. *International Journal of Remote Sensing*, **2**, 231–252.

LO, C. P., and NOBLE, W. E. Jr, 1990, Detailed urban land-use and land-cover mapping using Large Format Camera photographs: an evaluation. *Photogrammetric Engineering and Remote Sensing*, **56**, 197–206.

MCFEETERS, S. K., 1996, The use of the Normalized Difference Water Index (NDWI) in the delineation of open water features. *International Journal of Remote Sensing*, **17**, 1425–1432.

SIDJAK, R. W., and WHEATE, R. D., 1999, Glacier mapping of the Illecillewaet icefield, British Columbia, Canada, using Landsat TM and digital elevation data. *International Journal of Remote Sensing*, **20**, 273–284.

SLATER, M. T., SLOGGETT, D. R., REES, W. G., and STEEL, A., 1999, Potential operational multi-satellite sensor mapping of snow cover in maritime sub-polar regions. *International Journal of Remote Sensing*, **20**, 3019–3030.

STUCKENS, J., COPPIN, P. R., and BAUER, M. E., 2000, Integrating contextual information with per-pixel classification for improved land cover classification. *Remote Sensing of Environment*, **71**, 282–296.

TREITZ, P. M., HOWARTH, P. J., and GONG, P., 1992, Application of satellite and GIS technologies for land-cover and land-use mapping at the rural–urban fringe: a case study. *Photogrammetric Engineering and Remote Sensing*, **58**, 439–448.